scientific reports

Check for updates

OPEN

Increased coherence predicts medical refractoriness in patients with temporal lobe epilepsy on monotherapy

Sungeun Hwang[1,12], Youmin Shin[2,3,12], Jun-Sang Sunwoo[4], Hyoshin Son[5], Seung-Bo Lee[6], Kon Chu[7,8], Ki-Young Jung[7,8], Sang Kun Lee[7,8], Young-Gon Kim[2,9,11,12]✉ & Kyung-Il Park[8,10,12]✉

Among patients with epilepsy, 30–40% experience recurrent seizures even after adequate antiseizure medications therapies, making them refractory. The early identification of refractory epilepsy is important to provide timely surgical treatment for these patients. In this study, we analyze interictal electroencephalography (EEG) data to predict drug refractoriness in patients with temporal lobe epilepsy (TLE) who were treated with monotherapy at the time of the first EEG acquisition. Various EEG features were extracted, including statistical measurements and interchannel coherence. Feature selection was performed to identify the optimal features, and classification was conducted using different classifiers. Functional connectivity and graph theory measurements were calculated to identify characteristics of refractory TLE. Among the 48 participants, 34 (70.8%) were responsive, while 14 (29.2%) were refractory over a mean follow-up duration of 38.5 months. Coherence feature within the gamma frequency band exhibited the most favorable performance. The light gradient boosting model, employing the mutual information filter-based feature selection method, demonstrated the highest performance (AUROC = 0.821). Compared to the responsive group, interchannel coherence displayed higher values in the refractory group. Interestingly, graph theory measurements using EEG coherence exhibited higher values in the refractory group than in the responsive group. Our study has demonstrated a promising method for the early identification of refractory TLE utilizing machine learning algorithms.

Keywords Electroencephalography, Machine learning, Optimized feature selection, Prediction, Refractory epilepsy, Temporal lobe epilepsy

Epilepsy is a neurological disease characterized by recurrent seizures[1]. The primary treatment modality for epilepsy is anti-seizure medication (ASM) and regular maintenance of ASM is required to minimize seizure recurrence, even in patients who experience infrequent seizures.

Numerous cohort studies have revealed that optimal ASM provides seizure freedom in 60–70% of patients with newly diagnosed epilepsy[2]. That is, the remaining 30–40% experience recurrent seizures even after adequate ASM therapy and are therefore classified as having refractory epilepsy. The International League Against Epilepsy Task Force proposed a consensus definition of refractory (or drug-resistant) epilepsy as "failure of adequate trials of two tolerated and appropriately chosen and used ASM schedules (whether as monotherapies or in

[1]Department of Neurology, Ewha Womans University Mokdong Hospital, Seoul, Republic of Korea. [2]Department of Transdisciplinary Medicine, Seoul National University Hospital, Seoul, Republic of Korea. [3]Interdisciplinary Program in Bio-Engineering, Seoul National University, Seoul, Republic of Korea. [4]Department of Neurology, Kangbuk Samsung Hospital, Seoul, Republic of Korea. [5]Department of Neurology, Catholic University of Korea, Seoul, Republic of Korea. [6]Department of Medical Informatics, Keimyung University School of Medicine, Daegu, Republic of Korea. [7]Department of Neurology, Seoul National University Hospital, Seoul, Republic of Korea. [8]Department of Neurology, Seoul National University College of Medicine, Seoul, Republic of Korea. [9]Department of Medicine, Seoul National University College of Medicine, Seoul, Republic of Korea. [10]Department of Neurology, Seoul National University Hospital Healthcare System Gangnam Center, Seoul, Republic of Korea. [11]Innovative Medical Technology Research Institute, Seoul National University Hospital, Seoul, Republic of Korea. [12]These authors contributed equally: Sungeun Hwang, Youmin Shin, Young-Gon Kim and Kyung-Il Park. ✉email: younggon2.kim@gmail.com; ideopki@gmail.com

combination) to achieve sustained seizure freedom"[3]. This definition has been used to facilitate early identification of refractory epilepsy. Consequently, it encourages the exploration of alternative treatment modalities, including epilepsy surgery, neuromodulation, and ketogenic diet[4].

Ideally, the earlier the refractoriness is determined, the sooner epileptologists can consider alternative treatment options, such as surgery, in addition to rigorous medical treatment. Moreover, earlier resective surgery was correlated with better seizure outcome[5]. The likelihood of achieving seizure control decreases substantially with an increasing number of ASM trials[6]. Therefore, surgical treatment should be considered after failure of two adequate ASM regimens to achieve better seizure outcome. Seizures relapse in approximately 50% of patients after the failure of the first ASM regimen. Therefore, the early stages of ASM treatment are critical for identifying refractory epilepsy. For this purpose, researchers have used test results from drug-naïve patients to predict medical refractoriness. A previous study involving 287 drug-naïve patients incorporated clinical data, dichotomized imaging data, and EEG results[7]. However, individuals who used more than one ASM throughout the follow-up period were excluded from the study, potentially limiting the generalizability of the findings to a broader clinical population. Another study utilized claims data from a cohort of 582,258 patients to predict medical refractoriness[8]. However, in this study, refractory epilepsy was operationally defined as the prescription of more than four ASMs due to the paucity of information on seizure occurrence.

Another challenge in assessing refractoriness and the occurrence of seizures is the sole reliance on the patient's memory. Recent research has shown that more than half of focal impaired awareness seizures or nocturnal seizures go unnoticed and are not reported[9]. This underscores the need for objective tools such as electroencephalography (EEG) or imaging to observe the current status or predict refractoriness.

Several clinical factors, such as early onset of epilepsy, symptomatic or cryptogenic epilepsy, multiple seizure types, many seizures before ASM treatment, and a family history of epilepsy, have been reported to be associated with refractory epilepsy in previous studies[2,10]. In a recent meta-analysis, EEG abnormality was a consistent predictive factor for refractory epilepsy[11]. Both slow waves and epileptiform discharges have been associated with refractory epilepsy in newly diagnosed patients with epilepsy[12–14].

Recently, machine learning (ML) algorithms have been employed in patients with epilepsy. Researchers utilized ML algorithms to monitor seizure[15] or to predict epilepsy outcomes. Many researchers have used diverse features that were previously established by conventional statistical methods[7,16]. In these models, the EEG results were presented as categorical variables (i.e., normal, non-epileptiform abnormality, or epileptiform discharge). Presurgical clinical, electrographic, neuropsychological, imaging, and surgical data were used to predict surgical outcomes in patients with temporal lobe epilepsy[17,18]. Some studies utilized features from raw EEG data to predict treatment responses to levetiracetam[19,20]. However, only a few studies have used EEG-based features to predict medical refractoriness.

Lin et al. built an SVM model to predict medical refractoriness in 23 children with idiopathic epilepsy[21]. They extracted 24 EEG features from nine categories (autoregressive modeling predictive error, decorrelation time, energy, entropy, Hjorth, relative power, spectral edge, statistic, and energy of the wavelet coefficients). Gain ratio measure was adopted for feature selection. Wang et al. also developed an SVM model to predict medical refractoriness in a group of 164 drug-naive children and adults with epilepsy[22]. This model utilized a combination of clinical characteristics and EEG functional connectivity features (phase-lag index). For feature selection, RFE was applied. Although these studies used various features, only SVM classifier was utilized. Also, they included a heterogeneous group of patients with both focal and generalized epilepsy.

In an earlier study, the first ASM led to a seizure-free rate of 47%, the second ASM achieved a seizure-free rate of 13%, and the third option resulted in a seizure-free rate of only 4%[10]. Considering these statistics, patients who fail to reach a seizure-free status with initial monotherapy seem to have a likelihood of seizure freedom of less than 20% after further ASM trials. Therefore, we generated an ML model using EEG-based features to predict medical refractoriness in patients with temporal lobe epilepsy on initial monotherapy.

Results

Demographic and clinical characteristics

Forty-eight patients with unilateral TLE treated with monotherapy between 2014 and 2021 were identified; 33 (68.8%) patients had left-sided TLE, and 15 (31.3%) had right-sided TLE. The age of epilepsy onset was 44.9 ± 19.2 years old (mean ± standard deviation), and the age in the EEG study was 54.1 ± 15.5 years old. The follow-up duration from the EEG study to the last follow-up (when the final outcome was determined) was 38.5 ± 21.8 months. Of the 48 patients, 34 (70.8%) were responsive, and 14 (29.2%) were refractory to ASM treatment at the last follow-up. Hippocampal sclerosis was identified in 5 (10.4%) patients, trauma in 5 (10.4%) patients, and hemorrhage in 5 (10.4%) patients. The most frequently used ASM in the EEG study was levetiracetam (N = 20, 41.7%), followed by oxcarbazepine (N = 9, 18.8%) and lacosamide (N = 8, 16.7%). No demographic or clinical characteristics were significantly different between the responsive and refractory groups (Table 1). Length of EEG analyzed could be found in Supplementary Table S1.

Predictive performance across various frequency bands and features

The overall flowchart of the analysis is provided in Supplementary Fig. S1. Figure 1 shows the predictive performance of the responsive and refractory groups across different frequency bands using various features extracted from EEG signals. On average, features based on interchannel connectivity, such as Pearson's correlation coefficient and coherence, outperformed those derived from single-channel information, including the Hjorth parameter, statistical measures, energy metrics, and zero-crossing rate. In a comparative evaluation of the highest AUROC values among the various frequency bands and features, single-channel features yielded an average

	Responsive group (N = 34)	Refractory group (N = 14)	p-value
Sex (N, %)			0.830[a]
Male	19 (55.9%)	9 (64.3%)	
Female	15 (44.1%)	5 (35.7%)	
Age of epilepsy onset (years, mean ± s.d.)	45.4 ± 19.5	43.9 ± 19.0	0.809[b]
Age at EEG study (years, mean ± s.d.)	53.4 ± 16.7	55.9 ± 12.6	0.626[b]
Follow-up duration (months, mean ± s.d.)	39.0 ± 22.5	37.2 ± 21.0	0.800[b]
Seizure types (N, %)			0.810[a]
Focal seizures only	20 (58.8%)	7 (50.0%)	
Focal and focal to bilateral tonic–clonic seizures	14 (41.2%)	7 (50.0%)	
Etiology (N, %)			0.692[c]
Hippocampal sclerosis	3 (8.8%)	2 (14.3%)	
Trauma	4 (11.8%)	1 (7.1%)	
Hemorrhage	2 (5.9%)	3 (21.4%)	
Cerebral infarction	1 (2.9%)	1 (7.1%)	
Moyamoya disease	2 (5.9%)	0 (0.0%)	
Encephalitis	1 (2.9%)	1 (7.1%)	
Focal cortical dysplasia	1 (2.9%)	0 (0.0%)	
Cavernous malformation	1 (2.9%)	0 (0.0%)	
Unknown	19 (55.9%)	6 (42.9%)	
History of febrile convulsion (N, %)	2 (5.9%)	0 (0.0%)	0.895[c]
History of CNS infection (N, %)	1 (2.9%)	0 (0.0%)	1.000[c]
Epileptic focus (N, %)			0.441[a]
Left	25 (73.5%)	8 (57.1%)	
Right	9 (26.5%)	6 (42.9%)	
ASM at EEG study (N, %)			0.361[c]
Levetiracetam	16 (47.1%)	4 (28.6%)	
Oxcarbazepine	7 (20.6%)	2 (14.3%)	
Lacosamide	4 (11.8%)	4 (28.6%)	
Valproic acid	4 (11.8%)	1 (7.1%)	
Carbamazepine	2 (5.9%)	2 (14.3%)	
Lamotrigine	0 (0.0%)	1 (7.1%)	
Topiramate	1 (2.9%)	0 (0.0%)	
Seizure frequency at EEG study (per month, mean ± s.d.)	0.5 ± 1.7	0.6 ± 0.5	0.788[b]
IED on first EEG (N, %)	15 (44.1%)	10 (71.4%)	0.160[a]

Table 1. Demographic and clinical characteristics of the responsive and refractory groups. *EEG* electroencephalography, *s.d.* standard deviation, *ASM* antiseizure medication, *IED* interictal epileptic discharge, *CNS* central nervous system. [a]Chi-square test. [b]Mann−Whitney U test. [c]Fisher's exact test.

AUROC of 0.518, whereas interchannel features yielded an average AUROC of 0.611. Notably, the coherence feature with the gamma frequency attained the highest AUROC over the fivefold (0.635 ± 0.131).

Predictive performance across various machine learning models and feature selection methods

In the analysis of coherence features within the gamma frequency, which demonstrated the highest performance in Fig. 1, 190 features were extracted and subsequently analyzed. When implementing feature selection across various ML models, the optimal performance was achieved using the mutual information filter-based feature selection method, in conjunction with LGB (Fig. 2), with the extraction of 25 features. At the window level, the model exhibited an AUROC of 0.774 (95% CI 0.643–0.904), accuracy of 0.757 (95% CI 0.659–0.855), sensitivity of 0.667 (95% CI 0.457–0.876), specificity of 0.807 (95% CI 0.687–0.926), positive predictive value of 0.681 (95% CI 0.522–0.840), and negative predictive value of 0.818 (95% CI 0.726–0.910). Advancing to a patient-level evaluation via soft voting, an AUROC of 0.821 (95% CI 0.654–0.988), accuracy of 0.791 (95% CI 0.640–0.943), sensitivity of 0.683 (95% CI 0.389–0.977), specificity of 0.838 (95% CI 0.692–0.984), positive predictive value of 0.700 (95% CI 0.439–0.961), and negative predictive value of 0.855 (95% CI 0.724–0.985) were achieved. Of 31 external validation set, 18 (58.1%) were responsive and 13 (41.9%) were refractory to ASM treatment. For external validation set, an AUROC was 0.718 (95% CI 0.682–0.735) at the window level, and 0.798 (95% CI 0.747–0.829) at the patient level. For a comprehensive view of the performance metrics, refer to Table 2. Confusion matrix during fivefold could be found in Supplementary Fig. S2.

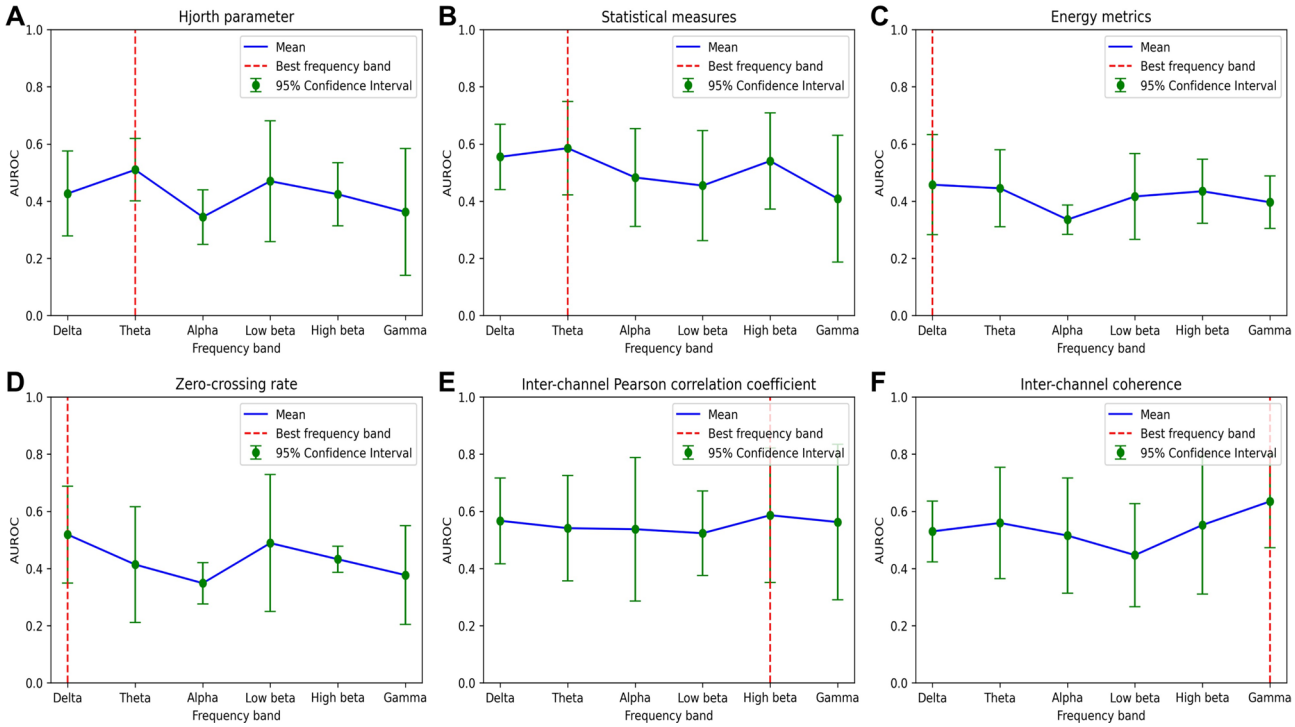

Fig. 1. Comparative prediction performance across various features. (**A**) Hjorth parameter. (**B**) Statistical measures. (**C**) Energy metrics. (**D**) Zero-crossing rate. (**E**) Interchannel Pearson correlation coefficient. (**F**) Interchannel coherence. The mean AUROC for each feature is indicated by a blue line, with the corresponding 95% confidence intervals depicted by green lines. A red vertical line marks the feature achieving the highest AUROC in each feature, highlighting the coherence feature within the gamma frequency band as the top performer with an AUROC of 0.635. *AUROC* average area under the receiver operating characteristic curve.

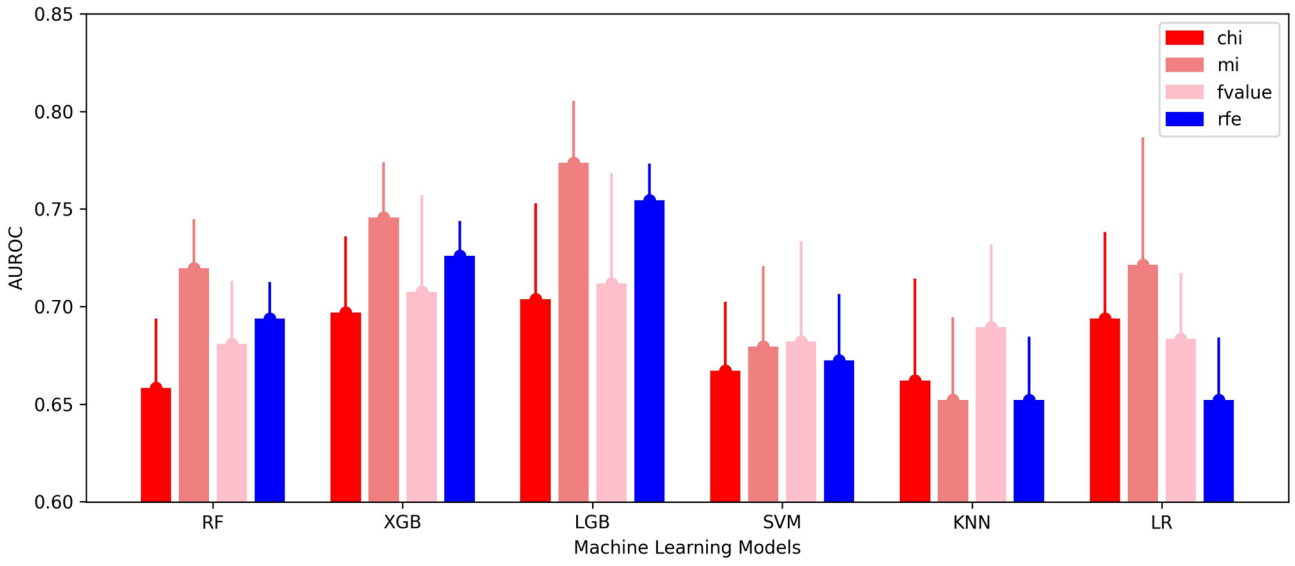

Fig. 2. Comparative analysis of prediction performance across different machine learning models and feature selection methods. The figure shows the area under the ROC curve (AUROC) for each model and feature selection method combination. Red and blue colors represent filter-based and wrapper-based feature selection methods, respectively. The analysis demonstrates the performance variability of models when using different feature selection techniques. Notably, the Light Gradient Boosting (LGB) model with mutual information filter-based feature selection achieved the highest AUROC of 0.774. This comparison highlights the significance of feature selection methods on model performance, guiding the selection of the most effective approach. *AUROC* average area under the receiver operating characteristic curve, *MI* mutual information, *ANOVA* analysis of variance, *RFE* recursive feature elimination, *RF* random forest, *XGB* extreme gradient boosting, *LGB* light gradient boosting, *SVM* suppor vector machine, *KNN* k-nearest neighbour's, *LR* logistic regression.

Dataset	Level	AUROC	Accuracy	Sensitivity	Specificity	PPV	NPV
Develop	Window	0.774 [0.643–0.904]	0.757 [0.659–0.855]	0.667 [0.457–0.876]	0.807 [0.687–0.926]	0.681 [0.522–0.840]	0.818 [0.726–0.910]
	Patient	0.821 [0.654–0.988]	0.791 [0.640–0.943]	0.683 [0.389–0.977]	0.838 [0.692–0.984]	0.700 [0.439–0.961]	0.855 [0.724–0.985]
External validation	Window	0.718 [0.682–0.735]	0.670 [0.644–0.675]	0.699 [0.633–0.744]	0.810 [0.763–0.837]	0.837 [0.802–0.853]	0.663 [0.613–0.692]
	Patient	0.788 [0.747–0.829]	0.735 [0.705–0.766]	0.632 [0.613–0.651]	0.697 [0.662–0.732]	0.737 [0.716–0.759]	0.585 [0.570–0.600]

Table 2. Detailed prediction performances at window and patient level. Values are presented with [95% confidence interval]. *AUROC* average area under the receiver operating characteristic curve, *PPV* positive predictive value, *NPV* negative predictive value.

Functional network analysis using EEG coherence values

For functional network analysis, only the top 20 features (i.e. coherence values between EEG channel pairs) consistently selected across the folds (≥ three times out of five folds) were used. These channel pairs are as follows: Cz-C3, F3-C3, F4-Cz, Fz-C3, Fz-C4, Fz-Cz, P3-C3, P3-Fz, Pz-C3, Pz-O2, Pz-P7, F3-Ca, Pf-Fp1, P4-Fz, Pz-Cz, Pz-Fz, Pz-O1, Pz-P3, P4-F4, and Pz-F4. The SHAP index and importance of the selected channel pairs observed across the five folds are illustrated in Supplementary Figs. S3 and S4, respectively. Supplementary Table S2 shows how many times each channel pair was selected during the folds. Coherence values of selected channel pairs at the window and patient levels are presented in Supplementary Tables S3 and S4.

Figure 3 presents a direct comparison of the top 20 selected channel pairs between the responsive and refractory groups at both window and patient levels. In particular, interchannel coherence displayed larger values in the refractory group (blue lines) than in the responsive group (red lines). Coherences with larger values in the responsive group were primarily observed in the hemisphere ipsilateral to the epileptic focus, which is represented as red edges in Fig. 3. Conversely, coherences with larger values in the refractory group were distributed across the contralateral hemisphere (depicted as blue edges in Fig. 3) as well as in the ipsilateral hemisphere. Notably, only one channel pair (Pz-P7) was selected from among the channel pairs that involved the temporal area.

Graph theory measurements based on EEG coherence values

Table 3 presents a comparison of graph theory measurements based on EEG coherence values between the responsive and refractory groups. At the window level, the modularity, closeness centrality, clustering coefficient, betweenness centrality, and degree coefficient were significantly higher in the refractory group. Similarly, at the patient level, the modularity, eigenvector centrality, clustering coefficient, betweenness centrality, and degree coefficient were significantly higher in the refractory group.

Discussion

In this study, we developed an ML model to predict medical refractoriness using the initial EEGs of patients with TLE who were on monotherapy. The best prediction performance was achieved by the coherence of the gamma frequency band by applying a mutual information filter-based feature selection method utilizing LGB.

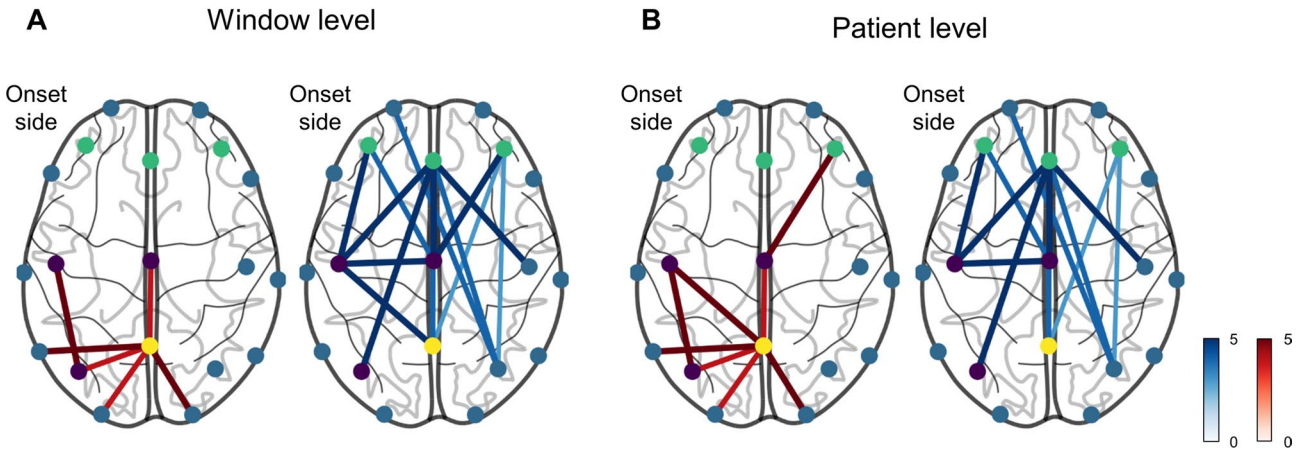

Fig. 3. Visualization of interchannel coherence value. Coherence values were demonstrated among selected channels at (**A**) window level and (**B**) patient level. Red edges indicate channel pairs with larger coherence values in the responsive group, and blue colors indicate channel pairs with larger coherence values in the refractory group. Note that the epileptic focus was placed in the left temporal area in this analysis. Visualizations were created using Python 3.9.12 with the Matplotlib 3.7.0 library. (https://matplotlib.org/3.7.0/).

Level	Graph measure	*p*-value	Responsive group (mean ± s.d.)	Refractory group (mean ± s.d.)
Window	Small worldness	0.636	1.042 ± 0.042	1.040 ± 0.041
	Modularity	< 0.001	0.136 ± 0.114	0.170 ± 0.096
	Eigenvector centrality	0.102	0.221 ± 0.043	0.226 ± 0.047
	Closeness centrality	< 0.001	0.260 ± 0.066	0.297 ± 0.032
	Clustering coefficient	< 0.001	0.323 ± 0.183	0.389 ± 0.181
	Betweenness centrality	< 0.001	0.062 ± 0.034	0.084 ± 0.025
	Degree coefficient	< 0.001	0.171 ± 0.087	0.200 ± 0.088
Patient	Small worldness	0.951	1.048 ± 0.048	1.047 ± 0.044
	Modularity	0.003	0.108 ± 0.104	0.208 ± 0.032
	Eigenvector centrality	0.032	0.216 ± 0.046	0.244 ± 0.024
	Closeness centrality	0.188	0.264 ± 0.066	0.295 ± 0.034
	Clustering coefficient	0.024	0.294 ± 0.195	0.442 ± 0.115
	Betweenness centrality	0.008	0.053 ± 0.037	0.086 ± 0.020
	Degree coefficient	0.022	0.156 ± 0.093	0.228 ± 0.052

Table 3. Graph measurement comparisons for patients with resting-state lengths exceeding 10 min at both window and patient levels. *s.d.* standard deviation.

The refractory group exhibited higher coherence values in the hemisphere contralateral to the epileptic focus than in the responsive group. In the graph analysis, the refractory group exhibited higher graph measurement values than the responsive group.

Among the various features analyzed in our study, coherence within the gamma frequency band demonstrated the most substantial predictive performance. Coherence, a measure of synchrony between EEG signals from different brain regions, offers valuable insights into brain functional connectivity. Disruptions in normal brain connectivity are the hallmark features of epilepsy. Our results align with this understanding, suggesting that higher coherence values in the gamma band may reflect altered or intensified neural communication, which is a characteristic feature of refractory epilepsy[23,24].

Notably, the refractory group exhibited higher coherence values than the responsive group, predominantly in the hemisphere contralateral to the epileptic focus. This observation may indicate compensatory or maladaptive network reorganization in refractory patients. The increased synchrony in the contralateral hemisphere may reflect the brain's attempt to counterbalance the disruption caused by epileptic activity in the affected hemisphere. However, this compensatory mechanism may contribute to the propagation of ictal discharges throughout the entire brain network. Consequently, the persistence or aggravation of seizures due to network alteration can lead to medical refractoriness.

Furthermore, the superior predictive performance of coherence over that of Pearson's correlation underscores the importance of considering frequency-specific brain connectivity measures in the study and management of epilepsy. Due to its sensitivity to frequency-specific synchronization relevant to epilepsy, coherence in the gamma frequency band has emerged as a more precise tool for predicting medical refractoriness[25–27].

Horstmann et al. identified higher clustering coefficients and average path lengths in patients with temporal or neocortical extratemporal epilepsy than in controls[28]. This distinction was particularly notable in the delta band. Van Diessen et al. studied various graph theory metrics (degree centrality, path length, clustering coefficient, betweenness centrality, closeness centrality, and eigenvector centrality) between children with focal epilepsy and controls[29]. Although none of the graph theory measurements showed significant differences between the two groups, an RF-based model utilizing these variables successfully distinguished children with focal epilepsy, achieving an AUROC of 0.89. Regarding the prediction of refractory epilepsy, Lee et al. observed a higher mean clustering coefficient within the hippocampal network in patients with refractory TLE than in those with responsive TLE[30]. Consistent with these findings, we observed altered graph theory parameters in the refractory group within our study population. Specifically, the modularity, eigenvector centrality, clustering coefficient, betweenness centrality, and degree coefficient were higher in the refractory group than in the responsive group.

This study has few limitations. (1) Small sample size. This study has a relatively small sample size of 48 patients. The limited sample size could be attributed to two factors. First, the EEG recordings were restricted to a single EEG system, which constrained the number of available subjects. Second, the study focused exclusively on patients with TLE, which contributed to a limited sample size. Therefore, future research may benefit from a multicenter approach and the application of transfer-learning techniques to overcome machine- and site-specific disparities. (2) Timing of EEG acquisition. EEG data were collected after the administration of the first ASM rather than before ASM initiation. This choice was predominantly influenced by the practical difficulty of conducting an EEG immediately after a seizure due to the extended waiting times in the institutions participating in this study. (3) Asymmetry of left and right hemisphere was not considered in adjustment of EEG signals from participants whose epileptic focus was in the right hemisphere. Functional differentiation of language and visuospatial domain exists in cerebral hemispheres, therefore EEG signals from left and right hemispheres are exactly symmetric. However, in this study, we were able to perform graph analyses in regards to epileptic focus because we flipped EEG signals from participants with right epileptic focus.

In this study, we developed an ML model to predict medical refractoriness in patients with TLE using EEG coherence features. By limiting the study subjects to patients with unilateral TLE, we were able to interpret the functional connectivity analysis results with respect to the epileptic focus. After initial diagnosis of TLE and initiation of single ASM, this ML model could help identify refractory TLE in referral hospitals, where most patients with refractory epilepsy are treated.

Methods

Patients and data collection

This is a retrospective observational study using routine clinical data. Adult patients (≥ 18 years) were enrolled at 2 tertiary referral centers for epilepsy, Seoul National University Hospital and Kangbuk Samsung Hospital between 2014 and 2021. Inclusion criteria were as follows: (1) TLE (temporal lobe epilepsy) diagnosis based on seizure semiology, EEG, and magnetic resonance imaging; (2) monotherapy (1 ASM) during the first EEG recording; (3) unilateral epileptic focus. For external validation, 31 TLE patients meeting the same inclusion criteria were enrolled from 2022 to 2023. Demographic and clinical characteristics, including baseline and final seizure frequencies, were obtained through a retrospective review of medical records. A total of 48 patients with TLE were selected and divided into two groups according to the final outcome, regardless of the final ASM regimen: the responsive group (no seizures during the last 1 year of follow-up) and the refractory group (one or more seizures in the last 1 year of follow-up) (Fig. 4).

Statistical analysis

We used the mean (standard deviation) or frequency (proportion) for statistical analyses. Normality tests were performed using the Shapiro–Wilk test. The chi-square test was used to compare the distributions of sex, seizure type, epileptic focus, and interictal epileptic discharge on the first EEG between the groups. Fisher's exact test was used to compare the distributions of the etiology of epilepsy, history of febrile convulsion, history of central nervous system infection, and ASM at the first EEG between the groups. Mann–Whitney U test was used to analyze the differences in age at epilepsy onset, age at EEG study, follow-up duration, and seizure frequency at the time of EEG study between the groups. p-value under the threshold of 0.05 was considered statistically significant.

EEG recording

Interictal EEG data were recorded using the NicoletOne® EEG system (Natus, San Carlo, CA, USA), in accordance with the international 10–20 electrode placement protocol, with a sampling frequency of 250 Hz, a hardware high-pass filter of 0.1 Hz, and a hardware low-pass filter of 500 Hz. To ensure optimal signal quality, the impedance of all electrodes was meticulously maintained below 10 kΩ. This study leveraged datasets from two separate organizations to foster a comprehensive analysis. To guarantee uniformity across datasets, only 19 channels (electrodes: Fp1, F7, T7, P7, F3, C3, P3, O1, Fp2, F8, T8, P8, F4, C4, P4, O2, Fz, Cz, and Pz) universally present in both organizations were incorporated into the analysis. EEG data without any stimulus recorded with eyes closed were utilized for this study.

Preprocessing

Based on the results of a previous study, a minimum data length of 2 min was deemed necessary to analyze significant epileptic seizure signals effectively[31]. Adhering to this guideline, several data windows were created from the individual patient data, each spanning 120 s with a 50% overlap. The increased dataset size helps mitigate overfitting that originates from small datasets, as the model is less likely to learn from the idiosyncrasies of a

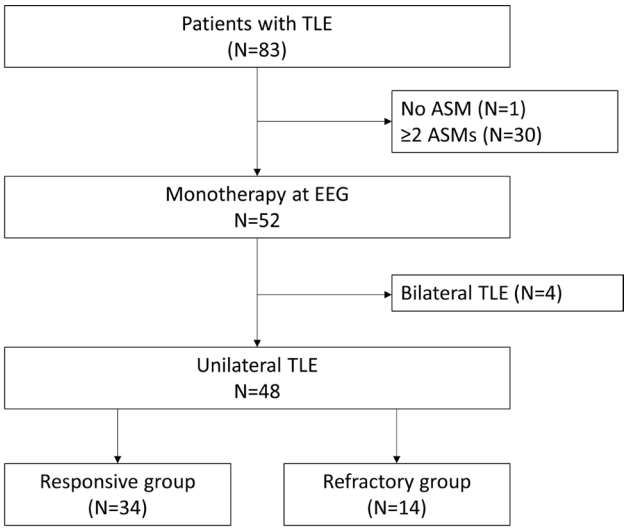

Fig. 4. Study flow diagram. *TLE* temporal lobe epilepsy, *ASM* antiseizure medication, *EEG* electroencephalography.

small dataset and more from generalizable patterns. Subsequently, the data were referenced from the average of the following EEG channels: F3, Fz, F4, C3, Cz, C4, P3, Pz, P4, O1, and O2.

To facilitate a nuanced analysis accounting for the initial site of a patient's epileptic seizures, a methodical strategy was employed to position the electrodes. For individuals with an epileptic focus on the left side, the existing EEG electrode placements were retained. Conversely, for those with an epileptic focus on the right side, the electrode positions were symmetrically adjusted. With this adjustment, the epileptic focus was positioned in the left hemisphere for each individual.

Prior to analysis, the signals underwent bandpass filtering across various frequency bands: delta (0.5–3 Hz), theta (3–8 Hz), alpha (8–12 Hz), low-beta (12–20 Hz), high-beta (20–30 Hz), and gamma (30–50 Hz), to segregate and highlight the relevant signal components for a more robust analysis.

Feature extraction

In the feature extraction phase, four time-domain features (Hjorth parameters, statistical measures, energy metrics, and zero-crossing rate) and two connectivity-based features (Pearson's correlation and coherence) were used for the analysis, owing to their proven significance in EEG analyses. In addition, connectivity analysis was conducted using Pearson's correlation and coherence analysis. To avoid duplication and to preserve analytical precision, connectivity values related to duplicated and symmetrically redundant information were omitted from the dataset.

(1) *Hjorth parameters* Hjorth parameters have been used to detect and diagnose seizures, as well as predict seizure recurrence after ASM withdrawal. This set encompasses three components: activity, which indicates the signal power; mobility, representing the mean frequency; and complexity, reflecting changes in frequency[32,33].
(2) *Statistical measures* Statistical parameters have been employed as features to differentiate patients with epilepsy from healthy controls and predict the response to levetiracetam[20,34]. Six prevalent statistical indicators were used as features: skewness, kurtosis, mean, median, minimum, and maximum values.
(3) *Energy metrics* Energy metrics serve as markers for assessing brain activity[35]. Therefore, the linear and nonlinear energies of the EEG signals were included to offer insights into the energy patterns present within the signal[36].
(4) *Zero-crossing rate* This parameter indicates the rate at which a signal transitions from positive to zero to negative or vice versa. It has been a prominent tool in numerous studies for distinguishing seizures from normal EEG signals. For this study, both the zero-crossing rate and its first derivative were incorporated into the analysis[37,38].
(5) *Interchannel Pearson's correlation coefficient* Pearson's correlation is a pivotal feature in brain analysis. It computes the linear relationship between two EEG channels and provides a measurement of both the strength and direction of the association between signal sets. This facilitates the identification of intricate patterns and potential anomalies within EEG signals[39–41].
(6) *Interchannel coherence* Coherence is a spectral-domain measure that offers insights into the synchrony between EEG channels in specific frequency bands. By evaluating the cross-spectral and auto-spectral densities, spectral-domain coherence facilitates the understanding of connectivity patterns and potential neural network alliances within EEG data[42,43].

Feature selection

Robust feature selection techniques were utilized to improve the performance of the ML model and reduce the risk of overfitting. Two principal methods were employed: filter-based and wrapper-based feature selection. It is critical to highlight that the feature selection process was confined exclusively to the training set. During our fivefold cross-validation procedure, we meticulously maintained a clear separation between the training and validation datasets. Feature selection was conducted exclusively using the training data. Subsequently, the performance metrics were evaluated solely based on the validation data for each fold.

(1) Filter-based feature selection is a technique that selects relevant features based on statistical properties. Three commonly used filter-based strategies (chi-square, ANOVA F-value, and mutual information) were employed[44]. Each of these methods was applied to assess the significance and contribution of individual features within our dataset.
(2) Wrapper-based method uses a search algorithm to evaluate different subsets of features and selects the optimal subset that achieves the best performance for a given ML model. Recursive feature elimination (RFE) was utilized as our wrapper method, systematically reducing the feature set to identify the most predictive features[45].

Evaluation

Six robust classifiers, random forest (RF)[46], extreme gradient boosting (XGB)[47], and light gradient boosting (LGB), support vector machine (SVM), K-nearest neighbors (KNN), logistic regression (LR) were employed in this study[48]. The optimal feature selection method was determined based on the average area under the receiver operating characteristic curve (AUROC) ascertained during a fivefold cross-validation process. A comprehensive assessment of the model's performance was facilitated through the analysis of various metrics, including the AUROC, accuracy, F1 score, sensitivity, and specificity. Moreover, both positive and negative predictive values

were meticulously scrutinized to gauge the proficiency of the model in accurately delineating the respective classes.

A fivefold cross-validation was implemented at the patient level, rather than at the individual window level. By implementing cross-validation at the patient level, all data pertaining to a single patient, including their respective windows, are grouped together. This ensures that the model is tested on completely unseen patients, providing a more reliable and accurate assessment of its ability to generalize and its true predictive power. After identifying the superior model and feature selection method at the window level, an evaluation at the patient level was conducted using a soft voting mechanism (Supplementary Fig. S5), which is a critical method for aggregating probabilistic predictions across each individual patient's window, thereby ensuring more nuanced, reliable, and comprehensive insights into the model's predictive capabilities.

Feature interpretation and graph measurement

The selected channel pairs may vary during the fivefold cross-validation process, highlighting the importance of focusing on channel pairs that are consistently chosen in at least three of the fivefold. The average feature importance and Shapley additive explanation (SHAP) values[49] for the chosen edges were systematically analyzed to understand their respective contributions to model predictions. Furthermore, a statistical comparative analysis was conducted between the responsive and refractory groups. A two-tailed paired *t*-test was employed to analyze each feature, both at the individual window levels and at the patient level (average window basis), with a significance threshold set at 0.05.

Given the prominence of coherence as a principal feature, the visualization results are depicted graphically. Each channel is represented as a node, and the coherence value is illustrated as an edge between the nodes. Graph visualization and analysis were performed using the NetworkX[50] and nilearn[51] Python libraries. To compare graph measurements, edges were connected in each window only if the coherence values were higher than 0.5. At the patient level, a single graph per patient was generated by averaging the values across all windows and subsequently connecting or disconnecting the edges based on a threshold of 0.5. Given the sensitivity of averaging to outliers, especially in cases with a limited number of windows, the analyses were restricted to patients with resting-state lengths exceeding 10 min, ensuring a minimum of 10 windows.

Data availability

The datasets generated during and/or analyzed during the current study are available from the corresponding author on reasonable request.

Received: 3 July 2024; Accepted: 29 August 2024
Published online: 04 September 2024

References

1. Fisher, R. S. *et al.* Instruction manual for the ILAE 2017 operational classification of seizure types. *Epilepsia* **58**, 531–542. https://doi.org/10.1111/epi.13671 (2017).
2. Chen, Z., Brodie, M. J., Liew, D. & Kwan, P. Treatment outcomes in patients with newly diagnosed epilepsy treated with established and new antiepileptic drugs: A 30-year longitudinal cohort study. *JAMA Neurol.* **75**, 279–286. https://doi.org/10.1001/jamaneurol.2017.3949 (2018).
3. Kwan, P. *et al.* Definition of drug resistant epilepsy: Consensus proposal by the ad hoc Task Force of the ILAE Commission on therapeutic strategies. *Epilepsia* **51**, 1069–1077. https://doi.org/10.1111/j.1528-1167.2009.02397.x (2010).
4. Brodie, M. J. & Sills, G. J. Combining antiepileptic drugs—Rational polytherapy? *Seizure* **20**, 369–375. https://doi.org/10.1016/j.seizure.2011.01.004 (2011).
5. Simasathien, T. *et al.* Improved outcomes with earlier surgery for intractable frontal lobe epilepsy. *Ann. Neurol.* **73**, 646–654. https://doi.org/10.1002/ana.23862 (2013).
6. Kwan, P. & Brodie, M. J. Epilepsy after the first drug fails: Substitution or add-on? *Seizure* **9**, 464–468. https://doi.org/10.1053/seiz.2000.0442 (2000).
7. Yao, L. *et al.* Prediction of antiepileptic drug treatment outcomes of patients with newly diagnosed epilepsy by machine learning. *Epilepsy Behav.* **96**, 92–97. https://doi.org/10.1016/j.yebeh.2019.04.006 (2019).
8. An, S. *et al.* Predicting drug-resistant epilepsy—A machine learning approach based on administrative claims data. *Epilepsy Behav.* **89**, 118–125. https://doi.org/10.1016/j.yebeh.2018.10.013 (2018).
9. Elger, C. E. & Hoppe, C. Diagnostic challenges in epilepsy: Seizure under-reporting and seizure detection. *Lancet Neurol.* **17**, 279–288. https://doi.org/10.1016/s1474-4422(18)30038-3 (2018).
10. Kwan, P. & Brodie, M. J. Early identification of refractory epilepsy. *N. Engl. J. Med.* **342**, 314–319. https://doi.org/10.1056/nejm200002033420503 (2000).
11. Xue-Ping, W., Hai-Jiao, W., Li-Na, Z., Xu, D. & Ling, L. Risk factors for drug-resistant epilepsy: A systematic review and meta-analysis. *Medicine* **98**, e16402. https://doi.org/10.1097/md.0000000000016402 (2019).
12. Aaberg, K. M. *et al.* Short-term seizure outcomes in childhood epilepsy. *Pediatrics* **141**, 16. https://doi.org/10.1542/peds.2017-4016 (2018).
13. Berg, A. T. *et al.* Early development of intractable epilepsy in children: A prospective study. *Neurology* **56**, 1445–1452. https://doi.org/10.1212/wnl.56.11.1445 (2001).
14. Ko, T. S. & Holmes, G. L. EEG and clinical predictors of medically intractable childhood epilepsy. *Clin. Neurophysiol.* **110**, 1245–1251. https://doi.org/10.1016/s1388-2457(99)00068-1 (1999).
15. Peng, G., Nourani, M., Harvey, J. & Dave, H. Personalized EEG feature selection for low-complexity seizure monitoring. *Int. J. Neural Syst.* **31**, 2150018. https://doi.org/10.1142/s0129065721500180 (2021).
16. Hakeem, H. *et al.* Development and validation of a deep learning model for predicting treatment response in patients with newly diagnosed epilepsy. *JAMA Neurol.* https://doi.org/10.1001/jamaneurol.2022.2514 (2022).
17. Grigsby, J., Kramer, R. E., Schneiders, J. L., Gates, J. R. & Brewster Smith, W. Predicting outcome of anterior temporal lobectomy using simulated neural networks. *Epilepsia* **39**, 61–66. https://doi.org/10.1111/j.1528-1157.1998.tb01275.x (1998).
18. Armañanzas, R. *et al.* Machine learning approach for the outcome prediction of temporal lobe epilepsy surgery. *PLoS ONE* **8**, e62819. https://doi.org/10.1371/journal.pone.0062819 (2013).

19. Zhang, J. H. *et al.* Personalized prediction model for seizure-free epilepsy with levetiracetam therapy: A retrospective data analysis using support vector machine. *Br. J. Clin. Pharmacol.* **84**, 2615–2624. https://doi.org/10.1111/bcp.13720 (2018).
20. Croce, P. *et al.* Machine learning for predicting levetiracetam treatment response in temporal lobe epilepsy. *Clin. Neurophysiol.* **132**, 3035–3042. https://doi.org/10.1016/j.clinph.2021.08.024 (2021).
21. Lin, L. C. *et al.* Early prediction of medication refractoriness in children with idiopathic epilepsy based on scalp EEG analysis. *Int. J. Neural Syst.* **24**, 1450023. https://doi.org/10.1142/s0129065714500233 (2014).
22. Wang, B. *et al.* An integrative prediction algorithm of drug-refractory epilepsy based on combined clinical-EEG functional connectivity features. *J. Neurol.* **269**, 1501–1514. https://doi.org/10.1007/s00415-021-10718-z (2022).
23. Matos, J. *et al.* Diagnosis of epilepsy with functional connectivity in EEG after a suspected first seizure. *Bioengineering* **9**, 690. https://doi.org/10.3390/bioengineering9110690 (2022).
24. Jiruska, P. *et al.* High-frequency network activity, global increase in neuronal activity, and synchrony expansion precede epileptic seizures in vitro. *J. Neurosci.* **30**, 5690–5701. https://doi.org/10.1523/jneurosci.0535-10.2010 (2010).
25. Engel, J. Jr., Bragin, A., Staba, R. & Mody, I. High-frequency oscillations: What is normal and what is not? *Epilepsia* **50**, 598–604. https://doi.org/10.1111/j.1528-1167.2008.01917.x (2009).
26. Fisher, R. S., Webber, W. R., Lesser, R. P., Arroyo, S. & Uematsu, S. High-frequency EEG activity at the start of seizures. *J. Clin. Neurophysiol.* **9**, 441–448. https://doi.org/10.1097/00004691-199207010-00012 (1992).
27. Pereda, E., Quiroga, R. Q. & Bhattacharya, J. Nonlinear multivariate analysis of neurophysiological signals. *Prog. Neurobiol.* **77**, 1–37. https://doi.org/10.1016/j.pneurobio.2005.10.003 (2005).
28. Horstmann, M. T. *et al.* State dependent properties of epileptic brain networks: Comparative graph-theoretical analyses of simultaneously recorded EEG and MEG. *Clin. Neurophysiol.* **121**, 172–185. https://doi.org/10.1016/j.clinph.2009.10.013 (2010).
29. van Diessen, E., Otte, W. M., Braun, K. P., Stam, C. J. & Jansen, F. E. Improved diagnosis in children with partial epilepsy using a multivariable prediction model based on EEG network characteristics. *PLoS ONE* **8**, e59764. https://doi.org/10.1371/journal.pone.0059764 (2013).
30. Lee, H. J. & Park, K. M. Intrinsic hippocampal and thalamic networks in temporal lobe epilepsy with hippocampal sclerosis according to drug response. *Seizure* **76**, 32–38. https://doi.org/10.1016/j.seizure.2020.01.010 (2020).
31. Shin, Y. *et al.* Using spectral and temporal filters with EEG signal to predict the temporal lobe epilepsy outcome after antiseizure medication via machine learning. *Sci. Rep.* **13**, 22532. https://doi.org/10.1038/s41598-023-49255-2 (2023).
32. Päivinen, N. *et al.* Epileptic seizure detection: A nonlinear viewpoint. *Comput. Methods Progr. Biomed.* **79**, 151–159. https://doi.org/10.1016/j.cmpb.2005.04.006 (2005).
33. Tanveer, M., Pachori, R. B. & Angami, N. V. Classification of seizure and seizure-free EEG signals using Hjorth parameters. In *2018 IEEE Symposium Series on Computational Intelligence (SSCI)* 2180–2185 (2018).
34. Gemein, L. A. W. *et al.* Machine-learning-based diagnostics of EEG pathology. *Neuroimage* **220**, 117021. https://doi.org/10.1016/j.neuroimage.2020.117021 (2020).
35. Lanzone, J. *et al.* The effect of Perampanel on EEG spectral power and connectivity in patients with focal epilepsy. *Clin. Neurophysiol.* **132**, 2176–2183. https://doi.org/10.1016/j.clinph.2021.05.026 (2021).
36. Ricci, L. *et al.* Measuring the effects of first antiepileptic medication in temporal lobe epilepsy: Predictive value of quantitative-EEG analysis. *Clin. Neurophysiol.* **132**, 25–35. https://doi.org/10.1016/j.clinph.2020.10.020 (2021).
37. Pyrzowski, J. *et al.* Zero-crossing patterns reveal subtle epileptiform discharges in the scalp EEG. *Sci. Rep.* **11**, 4128. https://doi.org/10.1038/s41598-021-83337-3 (2021).
38. ShahidiZandi, A., Tafreshi, R., Javidan, M. & Dumont, G. A. Predicting temporal lobe epileptic seizures based on zero-crossing interval analysis in scalp EEG. *Annu. Int. Conf. IEEE Eng. Med. Biol. Soc.* **2010**, 5537–5540. https://doi.org/10.1109/iembs.2010.5626764 (2010).
39. Morgan, V. L. *et al.* Magnetic resonance imaging connectivity for the prediction of seizure outcome in temporal lobe epilepsy. *Epilepsia* **58**, 1251–1260. https://doi.org/10.1111/epi.13762 (2017).
40. Antony, A. R. *et al.* Functional connectivity estimated from intracranial EEG predicts surgical outcome in intractable temporal lobe epilepsy. *PLoS ONE* **8**, e77916. https://doi.org/10.1371/journal.pone.0077916 (2013).
41. Peng, G., Nourani, M., Dave, H. & Harvey, J. SEEG-based epileptic seizure network modeling and analysis for pre-surgery evaluation. *Comput. Biol. Med.* **167**, 107692. https://doi.org/10.1016/j.compbiomed.2023.107692 (2023).
42. van Mierlo, P. *et al.* Functional brain connectivity from EEG in epilepsy: Seizure prediction and epileptogenic focus localization. *Prog. Neurobiol.* **121**, 19–35. https://doi.org/10.1016/j.pneurobio.2014.06.004 (2014).
43. Zaveri, H. P. *et al.* Localization-related epilepsy exhibits significant connectivity away from the seizure-onset area. *Neuroreport* **20**, 891–895. https://doi.org/10.1097/WNR.0b013e32832c78e0 (2009).
44. Chandrashekar, G. & Sahin, F. A survey on feature selection methods. *Comput. Electr. Eng.* **40**, 16–28. https://doi.org/10.1016/j.compeleceng.2013.11.024 (2014).
45. Guyon, I., Weston, J., Barnhill, S. & Vapnik, V. Gene selection for cancer classification using support vector machines. *Mach. Learn.* **46**, 389–422. https://doi.org/10.1023/A:1012487302797 (2002).
46. Breiman, L. Random Forests. *Mach. Learn.* **45**, 5–32. https://doi.org/10.1023/A:1010933404324 (2001).
47. Chen, T. & Guestrin, C. XGBoost: A scalable tree boosting system. In *Proc. 22nd ACM SIGKDD International Conference on Knowledge Discovery and Data Mining* (2016).
48. Ke, G. *et al. Neural Information Processing Systems.*
49. Lundberg, S. M. & Lee, S.-I. *Neural Information Processing Systems.*
50. Hagberg, A., Swart, P. & Chult, D. *Exploring Network Structure, Dynamics, and Function Using NetworkX* (Los Alamos National Lab, 2008).
51. Abraham, A. *et al.* Machine learning for neuroimaging with scikit-learn. *Front. Neuroinform.* **8**, 14. https://doi.org/10.3389/fninf.2014.00014 (2014).

Acknowledgements

This study was supported by a grant from the Korea Health Technology R&D Project through the Korea Health Industry Development Institute (KHIDI), funded by the Ministry of Health & Welfare, Republic of Korea (Grant Number: RS-2023-00265638).

Author contributions

S.H., Y.S., S.B.L., S.K.L., Y.G.K., and K.I.P. conceived and designed the study; S.H., J.S.S., and H.S. collected the data; S.H. and Y.S. conducted the analyses; S.H., Y.S., Y.G.K., and K.I.P. interpreted the data; S.H. and Y.S. wrote the manuscript; S.H., Y.S., J.S.S., H.S., S.B.L., K.C., K.Y.J., S.K.L., Y.G.K. and K.I.P. edited and approved the manuscript.

Competing interests
The authors declare no competing interests.

Ethical approval
This study was approved by the Institutional Review Board of Seoul National University Hospital (reference number H-2308-010-1455). The study was performed in accordance with the Declaration of Helsinki. Due to the retrospective nature of the study, the Institutional Review Board of Seoul National University Hospital waived the need of obtaining informed consent.

Additional information
Supplementary Information The online version contains supplementary material available at https://doi.org/10.1038/s41598-024-71583-0.

Correspondence and requests for materials should be addressed to Y.-G.K. or K.-I.P.

Reprints and permissions information is available at www.nature.com/reprints.

Publisher's note Springer Nature remains neutral with regard to jurisdictional claims in published maps and institutional affiliations.